PERGAMON

Quaternary Science Reviews 19 (2000) 1423–1436

QSR

# Seismic activity, inferred crustal stresses and seismotectonics in the Rana region, Northern Norway

Erik C. Hicks[a,b], Hilmar Bungum[a,b,*], Conrad D. Lindholm[a]

[a]*NORSAR, Box 51, N-2027 Kjeller, Norway*
[b]*Department of Geology, University of Oslo, Box 1047 Blindern, N-0316 OSLO, Norway*

**Abstract**

The seismotectonic significance of the Rana region is known both from the fact that this was the location of the largest known earthquake in Fennoscandia in recent times, the $M_S$ 5.8–6.2 earthquake of August 31, 1819, and from its relatively high, constant seismic activity also in the 20th century. In order to study this region in more detail, a local seismic network has been in operation there since July 1997, as part of the NEONOR (Neotectonics in Norway) project. The network was primarily designed to detect possible activity on the Båsmoen fault which runs $\sim$ 50 km subparallel to the Rana fjord, and which shows signs of likely post glacial activity. The results have revealed a quite complex spatio-temporal distribution of seismic activity, and has also shown no activity on the Båsmoen fault itself. During the first 18 months of operation (July 1997–January 1999), the network has detected 373 locatable seismic events, of which 267 were local earthquakes. Most of these earthquakes occurred in five groups in the western parts of the network. All five groups had similar NNW-ESW trends in epicenter locations, and all have shallow foci (2–12 km), similar to what has also been found earlier for other concentrated earthquake zones in Northern Norway, and the magnitude range is between $M_L$ 0.1 and 2.8. Earthquake focal mechanism solutions within the network reveal a predominance for normal faulting with the tensional stress axis perpendicular do the coastline (implying an unusual coast-parallel orientation of the principal horizontal compressive stress). The earthquakes occur in a region of maximum post-glacial uplift gradients, which supports deglaciation flexure as a viable explanation for these earthquakes. A certain influence from more local factors, however, tied in general to crustal in homogeneities, cannot be ruled out. 

## 1. Introduction

The Fennoscandian shield has long been recognized as an ideal natural laboratory for studies of lithospheric and asthenospheric response to glacial loading and unloading, on the basis of its history of glaciations and deglaciations, including an uplift rate today of 7 mm/yr in the Bothnian Bay region (e.g., Ekman, 1996; Fjeldskaar, 1994, 1997). The last deglaciation, which occurred of the order of 8–10,000 yr ago, was rapid but also most likely irregular (e.g., Denton and Hughes, 1981), in time as well as in space. As late as in the 1970s (Lundquist and Lagerbäck, 1976), strong manifestations of sudden crustal response to this deglaciation (Johnston, 1987) were found as prominent Lappland neotectonic faults indicating the early Holocene occurrence of several M7 + earthquakes in this region (Muir-Wood, 1989b; Bungum and Lindholm, 1997). While a broad range of research efforts on these topics were initiated in Sweden in the 1980s (e.g., Bäckblom and Stanfors, 1988), more recent neotectonic research on the Norwegian side has further contributed to our understanding of this phenomenon (e.g., Dehls and Olesen, 1998, 1999; Dehls et al., 2000).

The seismicity and seismotectonics along the continental margin and the coastal region of mid and northern Norway (Fig. 1) is well documented. Byrkjeland et al. (2000) and Fejerskov and Lindholm (2000) have recently studied the seismotectonics of this region in relation to possible stress generating mechanisms, and have concluded that even though the first-order regional compressive stress field most likely is connected to plate boundary-related ridge push forces, the ridge push stress effects in themselves are not considered sufficient for releasing earthquakes. These authors therefore claim that other regional and local stress factors, such as flexural stresses from sedimentary loading, together with favorably oriented and sufficiently weak faults, have to be invoked in order to explain the occurrence and distribution of earthquakes in this region.

* Correspondence address. NORSAR, P.O. Box 51, N-2007, Kjeller, Norway. Tel.: 47-6380-5900; fax: 6381-8719.
*E-mail address:* hilmar.bungum@norsar.no (H. Bungum).

0277-3791/00/$ - see front matter 
PII: S0277-3791(00)00071-8

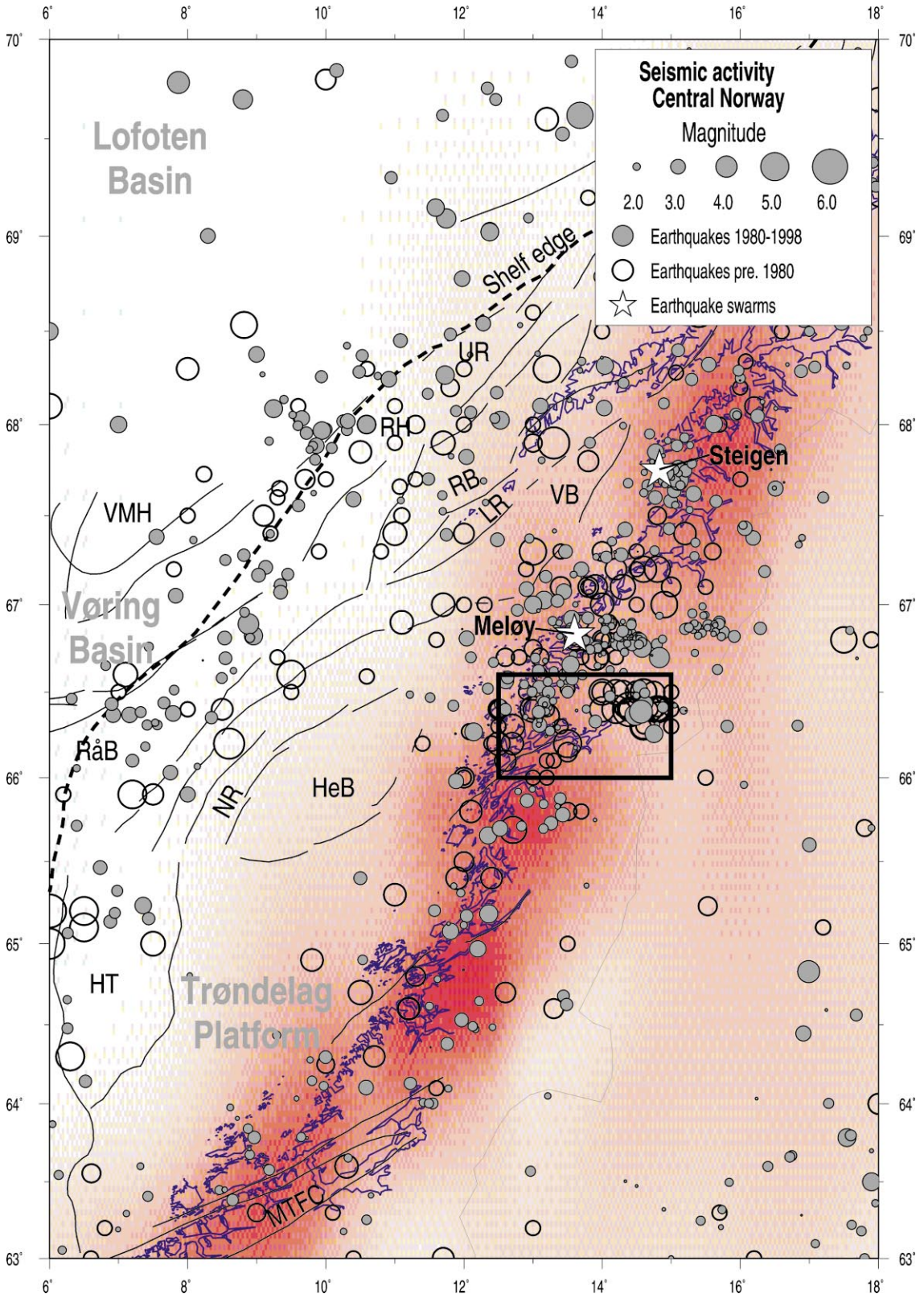


Fig. 1. Regional seismic activity from pre-1980 (open circles) and 1980 to 1998 (grey circles), from the NORSAR catalog (NORSAR and NGI, 1998). The black rectangle indicates the Rana area studied in this paper. The Meløy (Bungum et al., 1979) and Steigen (Atakan et al., 1994) earthquake swarms are shown by white stars. The uplift gradients calculated from a rather coarsly filtered grid (100 km lowpass) are shown in red, where dark red indicates a high uplift gradient. Structural information from Byrkjeland et al. (2000). HeB = Helgeland Basin, HT = Halten Terrace, LR = Lofoten Ridge, MTFC = Møre-Trøndelag Fault Complex, NR = Nordland Ridge, RB = Ribban Basin, RH = Røst High, RåB = Rås Basin, UR = Utrøst Ridge, VB = Vestfjorden Basin, VMH = Vøring Marginal High.

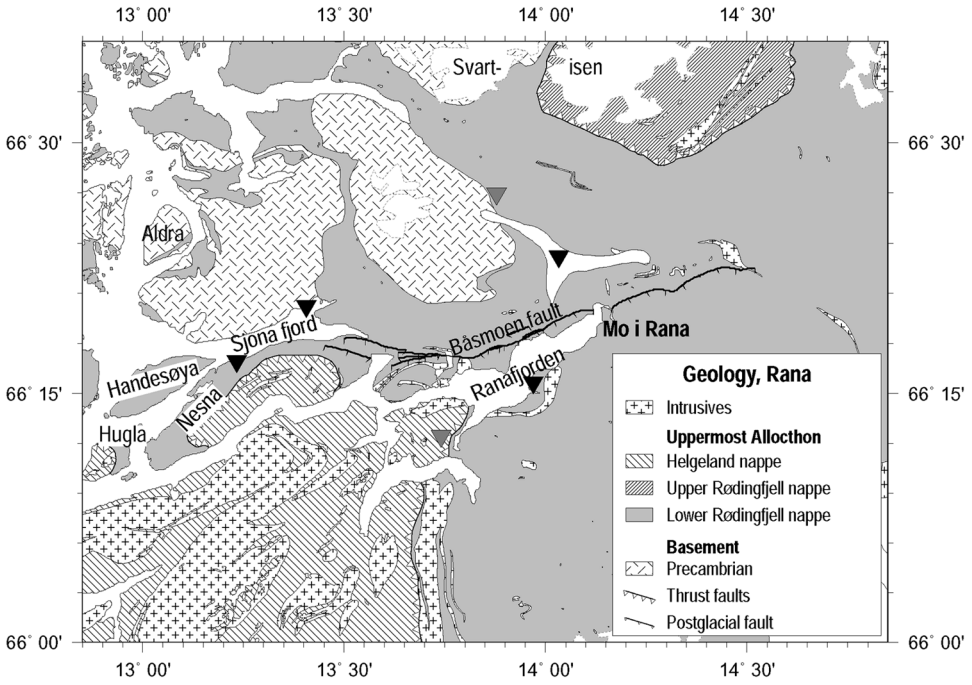


Fig. 2. Geological map of the Rana area, with seismic stations in the new local network included (inverted triangles). The two stations shown in grey were dismantled in September 1998. The Caledonian thrust belts in the Rana area are part of the Uppermost Allocthon, consisting mainly of mica-rich shales with granittic intrusions. The Precambrian basement mostly consists of granitic gneisses.

It is this seismicity along the coastal region of northern Norway which is the main subject of the present study. The main data used in pursuing this have been obtained from a local network of six short-period vertical-component stations which were installed in the Rana region in July 1997, extending about 40 km E–W and 25 km N–S (Fig. 2), and reduced to a four-station configuration in September, 1998. The purpose of this paper is to report the main results and to analyze and discuss them in a wider neo- and seismo-tectonic context.

## 2. Seismo-geological setting

### *2.1. Regional and local seismicity*

The seismicity distribution as shown in Fig. 1 has been established based on a combination of felt-area-based historical data (Muir-Wood and Woo, 1987) and more recent instrumental data using the country-wide network of seismic stations. In going from west to east towards the coast, Byrkjeland et al. (2000) have concluded that the oceanic crust is mostly aseismic apart from areas that have experienced rapid glacial loading since 2.6 Ma, notably in the East Lofoten and east Norway basin provinces. Here, thick sediment load and high deposition rates are considered to be responsible for local flexures and corresponding earthquake activity. The Vøring marginal high and the adjacent basins that experienced rifting and crustal thinning prior to the Early Tertiary continental breakup are almost entirely aseismic, suggesting that the crustal thickening and underplating resulting from the igneous breakup event have strengthened the crust in these regions.

Along the shelf edge (shown on Fig. 1), the seismicity is significant again, revealing a spatial correlation with a late Pliocene–Pleistocene glacial wedge which suggests that rapid sediment loading here has led to rejuvenation of Late Jurassic–Early Cretaceous faults. East of the main glacial wedge most of the seismic activity is found along the coast. Even if the post-glacial rebound is small in the coastal region the relative subsidence west of the hinge line makes the coastal region an area of high post-glacial rebound gradients, which implies high strains and increased seismicity.

Through the last of the above points we are in the focus area for the present study. NEONOR, a 1997–1999 neotectonics research project (Dehls and Olesen, 1998, 1999, 2000) selected the Rana area for a more in-depth study of a smaller region. Among the reasons for this was the fact that for a long time this region has revealed a relatively high, constant level of seismic activity, including the largest known historical earthquake in northwestern Europe, an M 5.8–6.2 earthquake in 1819 (Muir-Wood, 1989a), and that this region contains the prominent EW trending Båsmoen fault which has been considered to be likely neotectonic (Olesen et al., 1994; Dehls and Olesen, 1998).

The seismicity map in Fig. 1 shows, besides the seismicity along the shelf edge (which should be expected to relate to other stress generating mechanisms), that there also is a clear coastal trend, with the majority of the activity concentrated between 66 and 68°N. It is also seen in Fig. 1 that also the post-glacial uplift gradients are highest along the coast.

### 2.2. Local geological setting

The geology of the Rana area is dominated by the exotic terranes of the upper parts of the Caledonian thrust belts, emplaced towards the end of the Caledonian orogeny around 400 Ma, with smaller windows of Precambrian basement (Fig. 2). The nappes consist mainly of fairly high-grade metamorphic mica-rich shales, containing marble and large, mostly granitic intrusions. The lower units (lower and upper Rødingfjell nappes) occur to the north and west of the Rana area, and contain large marble bodies and moderately large granitic intrusions. The uppermost unit (Helgeland nappe) is found to the southwest of the Rana fjord, and is dominated by batholitic scale granitic instrusives, and is considered to originate from the western Laurentian continental margin. The visible Precambrian basement areas northwest of the Rana and Sjona fjords are mostly comprised of granitic gneisses.

Deglaciation of the Rana area occurred around 11000–9000 BP, constrained by mapping of moraine ridges (e.g. Blake and Olsen, 1999). The Vega glacial limit ( $\sim$ 12200 BP) Rasmussen, 1981; Gjelle et al., 1995) is only encountered offshore on islands west of the mainland, while the moraines associated with the Tjøtta glacial event (11200–10400 BP) can be followed across the mainland north of the Sjona fjord, across the Handnesøya and Hugla islands, and continue south of the Rana fjord (Andersen, 1975; Andersen et al., 1982, 1995). The Nordli (10200–10100 BP) moraines are located around 20 km east of the Tjøtta moraines (Andersen et al., 1982). The Preboreal moraines are quite poorly constrained between the Rana fjord and the Svartisen glacier, but several segments are mapped south of the Rana fjord that have been constrained in two groups that are correlated with the Narvik II and Rombak events (Bergstrøm, 1994; Olsen et al., 1996). The outer Preboreal moraine group consists of Narvik II (9600 $\pm$ 200 BP) south of the Svartisen glacier, (Andersen, 1975; Andersen et al., 1995) and is located around 15–20 km east of the Nordli moraines. The inner Preboreal moraine group, the Rombak moraines (9300 $\pm$ 200 BP) is located east of the Svartisen glacier to the north, and appears to pass quite close to Mo i Rana (Andersen, 1975; Andersen et al., 1995).

The Båsmoen fault is a southward-dipping reverse structure, from which the surface trace can be followed as a marked dip in the topography for around 50 km on the north side of the Rana fjord (Olesen et al., 1994). Studies performed as part of the NEONOR project concluded that the fault most likely has experienced post-glacial movement on the order of 30–40 cm, confined by C14 dating from layers directly above and below the tectonic indicators to between 8780 ( $\pm$ 80) and 3880 ( $\pm$ 75) yr BP (Dehls and Olesen, 2000).

### 2.3. Sources of stress

For the region under study there are three main sources of stress to be considered, namely the ridge push effect, density and differences (including topography) and flexural stresses (loading/unloading). In oceanic lithosphere, the ridge push force is considered capable of giving rise to stresses of the order of 20–30 MPa, dependent on (increasing with) age (Dahlen, 1981; Bott and Kusznir, 1984). Since the magnitude of stress is inversely proportional to the crustal thickness one should expect lower values ( $\sim$ 10–20 MPa) in thicker continental crust (Bott, 1991; Fejerskov and Lindholm, 2000), albeit dependent on possible subcrustal density differences. However, it is generally accepted (e.g., Byrkjeland et al., 2000) that the ridge push force in itself is not sufficient to explain the seismicity along the continental margin. This follows from the observation that the seismic activity is unevenly distributed, but follows tectonic features (including the margin itself, sedimentary depocenters, failed continental rifts, and the coast line), which identifies these structures as important. In addition, the inferred stress directions (Lindholm et al., 1995; Hicks et al., 2000) reveal significant deviation from the expected ridge push direction in the vicinity of the margin (shelf edge) and the coast, stabilizing again to that direction farther into the continent (Bungum et al., 1991; Gregersen, 1992; Zoback, 1992).

Among second-order sources of stress (Fejerskov and Lindholm, 2000) are lateral density contrasts, topography and its possible compensation at depth, changes in crustal thickness, and flexural loading and unloading. Loading effects may induce large flexural stresses ( $>$ 100 MPa), perturbing the regional stress field at wavelengths that however depend on the lateral extent of the load (e.g., Walcott, 1970; McNutt and Menard, 1982). The density contrast across the continent–ocean boundary causes extension normal to the margin within the continental lithosphere, and margin-normal compression in the oceanic lithosphere (Bott and Dean, 1972; Fejerskov and Lindholm, 2000), which is difficult to separate from the ridge push effect. At marginal highs, crystalline basement blocks should be expected to introduce tensional stresses within the high and compressive stresses on either side. Second-order stress effect of these kinds are therefore quite complicated and sensitive to local geological conditions.

While it is accepted that sediment loading may create large stresses ( $\sim$ 100 MPa) on passive margins (Frohlich, 1982; Stein et al., 1989), albeit with strong influence from the geometry of the load (e.g., Muir-Wood, 1993), the residual effects of glacial loading and unloading are more disputed (cf. Stephansson, 1988; Stein et al., 1989; Johnston et al., 1994). Essential parameters are the boundary conditions determined by the glacial loading history and in particular the plate relaxation time, where there are important differences between the models of Stephansson (1988) and Stein et al. (1989). The latter model is predicting deglaciation flexure with continental extension and oceanic compression, of the order of 10 MPa, and some support for this is found from the fact that observations indicate a change from *somewhat more* normal faulting toward land as compared to *somewhat more* thrust faulting seaward both on the Norwegian and Canadian margins (Adams and Basham, 1991; Hicks et al., 2000). To further complicate these considerations, however, there are indications that the response to glacial loading/unloading may be quite sensitive to the overburden conditions (Wu and Hasegawa, 1996), while Johnston et al. (1998) points to the importance of the lateral extent of the Fennoscandian ice sheet.

The regional characteristics of the Fennoscandian post-glacial uplift over time as well as at present is fairly well known. Much less is known, however, about local tectonic responses to this regional uplift. There is direct geodetic evidence that the spatial pattern of uplift may be more irregular than previously assumed (Olesen, 1988; Muir-Wood, 1993; Dehls and Olesen, 1999), and it is likely that the present-day seismicity is particularly sensitive to crustal irregularities (such as density differences, topography and weakness zones), as suggested by recent seismotectonic research concerned with this region (Fejerskov and Lindholm, 2000; Byrkjeland et al., 2000). Even though the passive continental margin in itself is important, as evidenced by global comparisons (Johnston and Kanter, 1990), the seismicity variation both along and across the margin is such that regional and local factors must have significant importance, including but not limited to the regional post-glacial uplift. Other factors of great importance are zones of weakness, including shear zones and pre-existing faults with favorable orientations with respect to the stress field, a situation which in turn is complicated by a poorly known distribution of crustal fluids (Sibson, 1995).

Our understanding of the seismicity of Norway has developed gradually in parallel with an improved instrumental coverage of the region (Havskov et al., 1992). The coastal areas of central Norway, particularly the northern parts, have long been known to exhibit relatively high levels of seismic activity, including several earthquake swarms, as discussed in more detail below, where yet another swarm area is identified, this time in Rana.

## 3. New microseismicity results

Between July 1997 and January 1999 a total of 373 seismic events (309 earthquakes) have been located using data from the new microseismicity network in Rana. 42 of the located events occurred within distances of 50–200 km from the network, and are thus outside the main study area. A total of 64 events have been classified as probable explosions, essentially on the basis of their time-of-day distribution and/or their occurrence in known areas of industrial activity, and therefore removed from the maps. The explosions mainly originate from a talc mine (Altermark mine) a few km northwest of Mo i Rana, and from Storforshei mines around 30 km east of Mo i Rana (mines in the area are shown in Fig. 5). This leaves 267 probable local earthquakes as a basis for this analysis. Fig. 3 shows the distribution of these earthquakes in and around in Rana fjord area.

### 3.1. Earthquake locations

There are five major groups of earthquake epicenters to be seen in Fig. 3, all in the western part of the network, and all with similar NNW–SSE trending distributions of epicenter locations. Even though there are no mapped faults which these earthquakes easily can be tied to, there are morphological lineations in that direction.

The group located under the eastern part of the Sjona fjord consists of 59 small earthquakes (magnitudes up to $M_L$1.6, using the scale of Alsaker et al., 1991) with the bulk of the activity in August to October, 1997. There has been only sporadic activity since then. The focal depths in this group are among the shallowest observed, mainly between 4 and 6 km. The group in the western part of the Sjona fjord (31 earthquakes) occurred mainly during November and December, 1997. The magnitudes are slightly higher here than in the first group, up to $M_L$1.8 and the earthquakes occur at slightly greater depths, 8–12 km.

The group further north, just south of the Aldra island (north of the Sjona fjord) was active mainly in January and February, 1998, although there was some sporadic activity also in 1997. 27 earthquakes make up this group, including the largest earthquake within the network during the period of operation, with a magnitude of $M_L$2.8. The hypocenter depths in this group lie in the 10–12 km range. A somewhat smaller group is located north of the three previous groups, containing two earthquakes with magnitudes of $M_L$2.1 and 2.3, in addition to 18 smaller earthquakes (magnitudes up to $M_L$1.2).

The fifth group consists of 51 earthquakes that occurred close to Handnesøya in October and December, 1998. The largest earthquake in this group had a magnitude of $M_L$2.7, and several of the larger events were felt by local inhabitants associated with banging/cracking noises. This implies very shallow hypocenter depths, of

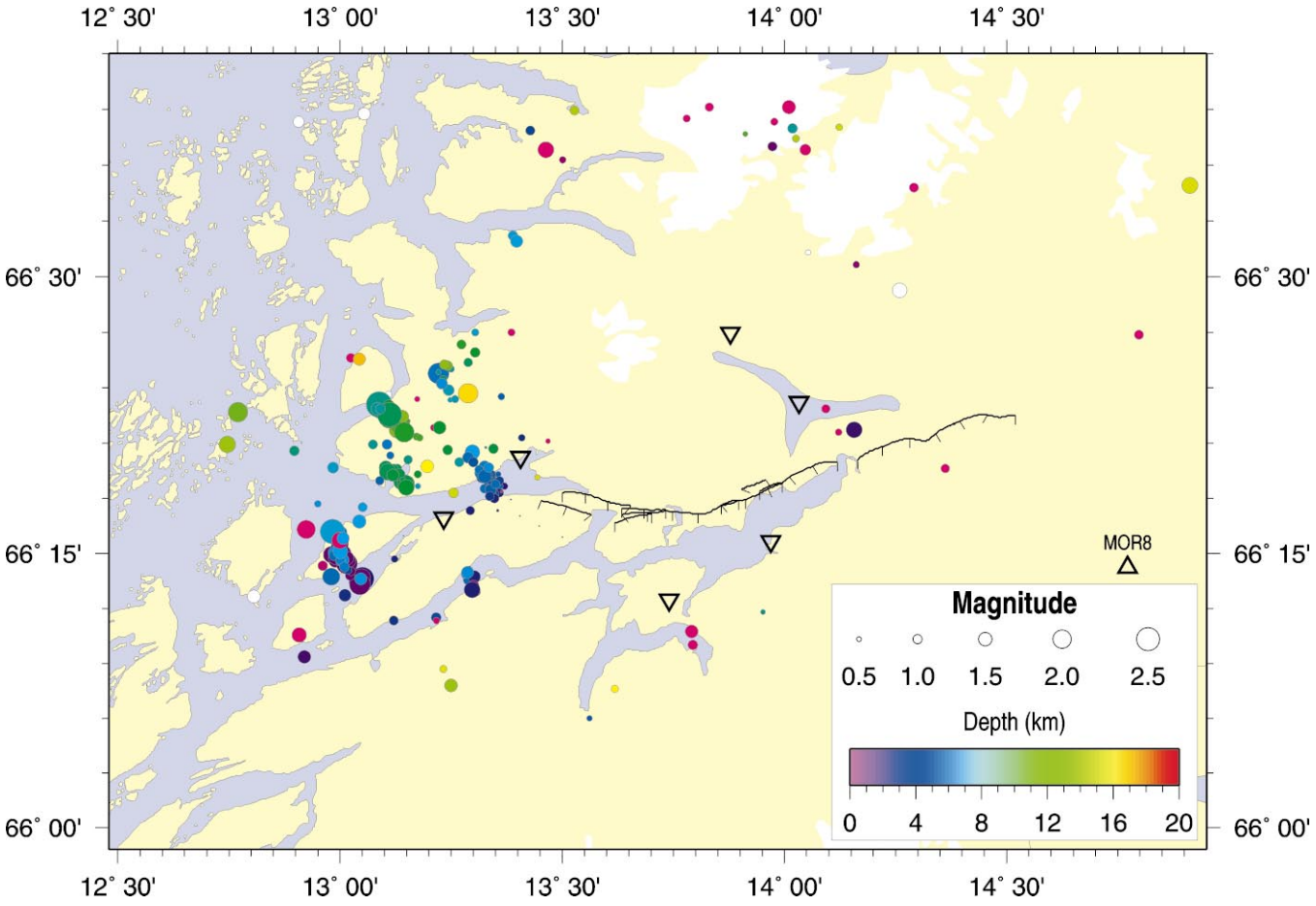


Fig. 3. Earthquakes located by the network August 1997–January 1999, plotted with symbol size proportional to magnitude ($M_L$) and color according to depth. Note the five main groups in the western parts of the map. These five groups include a majority of earthquakes in the Rana area. The MOR8 station in the eastern part of the map is part of the Norwegian national seismic network, data from this station have been used in the locations where available.

the order of only a few kilometers. The event locations yield hypocenter depths between 6 and 8 km.

The remaining local epicenters are quite scattered, with some of the largest ones being located under the Rana fjord on the southern side of the Nesna peninsula. There are also a few relatively large events further west, and a number of events are moreover located near the Svartisen glaciers north of Mo i Rana. There was also a single 'large' ($M_L$ 2.8) earthquake about 30 km south of the network, in an otherwise quiet area.

### 3.2. Focal mechanisms and inferred crustal stress

Of the 267 local earthquakes detected and located within the study area, a total of eight were of a quality which allowed the determination of focal mechanisms using data from the network. In addition, one composite solution using first motion polarities from 10 earthquakes in the eastern Sjona fjord group has been determined. The other eight solutions were determined using waveform modeling (Herrmann and Wang, 1985; Herrmann, 1987), which was essentially used to select a final solution after constraining the solution using available first motion polarities. All nine solutions are listed in Table 1 and shown in Fig. 4, where all solutions are also plotted together in terms of $P$ and $T$ axes, and as a rose diagram for the directions of the $P$ axes, trending NNE–SSW, and in terms of their faulting regime in a triangle plot (Frohlich and Apperson, 1992). It is seen there that all solutions except for two are found on the normal to strike-slip side. Fig. 4 finally shows an example of a real and the matching synthetic waveform for one of the focal mechanism solution (97.12.26, $M_L$ 1.8).

The maximum horizontal compressive stress directions ($\sigma_{Hmax}$ inferred from the focal mechanisms are plotted in Fig. 5, along with available in situ stress measurements from the region (Fejerskov et al., 1996). Even though a focal mechanism solution does not necessarily represent the true (precise) stress tensor (See e.g., McKenzie, 1969), it is well known that the stress directions derived from earthquake focal mechanism

Table 1
Earthquake focal mechanism solutions[a]

| Date | Lat. | Lon. | Depth (km) | Mag. ($M_L$) | $P$ trnd | $P$ plng | $T$ trnd | $T$ plng | Mode of faulting |
|---|---|---|---|---|---|---|---|---|---|
| Comp.1 | 66.31 | 13.32 | 5 | N/A | 167 | 48 | 270 | 11 | N–SS |
| 97.11.21 | 66.41 | 13.22 | 7 | 2.3 | 208 | 29 | 302 | 7 | SS |
| 97.11.25 | 66.50 | 12.40 | 11 | 2.7 | 77 | 29 | 343 | 7 | SS |
| 97.11.28 | 66.32 | 13.14 | 11 | 1.7 | 74 | 58 | 299 | 23 | NO |
| 97.11.28 | 66.32 | 13.15 | 11 | 1.8 | 74 | 58 | 299 | 23 | NO |
| 97.12.26 | 66.32 | 13.11 | 11 | 1.8 | 176 | 1 | 268 | 67 | R |
| 98.01.08 | 66.37 | 13.13 | 13 | 2.2 | 27 | 33 | 284 | 19 | SS–N |
| 98.02.09 | 66.39 | 13.09 | 11 | 2.8 | 351 | 22 | 257 | 11 | SS |
| 98.03.09 | 65.85 | 13.53 | 7 | 2.8 | 115 | 13 | 225 | 57 | RO |

[a]The composite solution is based on first-motion polarities from 10 earthquakes ($M_L$ 0.9–1.6). All eight single-event solutions are determined from waveform modelling constrained by first-motion polarities. $P_{trnd}$, $P_{plng}$, $T_{trnd}$ and $T_{plng}$ are trend and plunge of $P$ (Compression) and $T$ (tension) axes, respectively. The earthquakes dated 97.11.25 and 98.03.09 have locations outside the network. The modes of faulting N = normal, No = normal oblique, R = reverse, RO = reverse oblique, SS = strike-slip) correspond to the locations of the solutions in the triangle plot in Fig. 4, where pure normal, reverse and strike-slip (indicated circle sectors) requires a plunge of at least 60° of the $P$, $T$ and $B$ (null) axes, respectively.

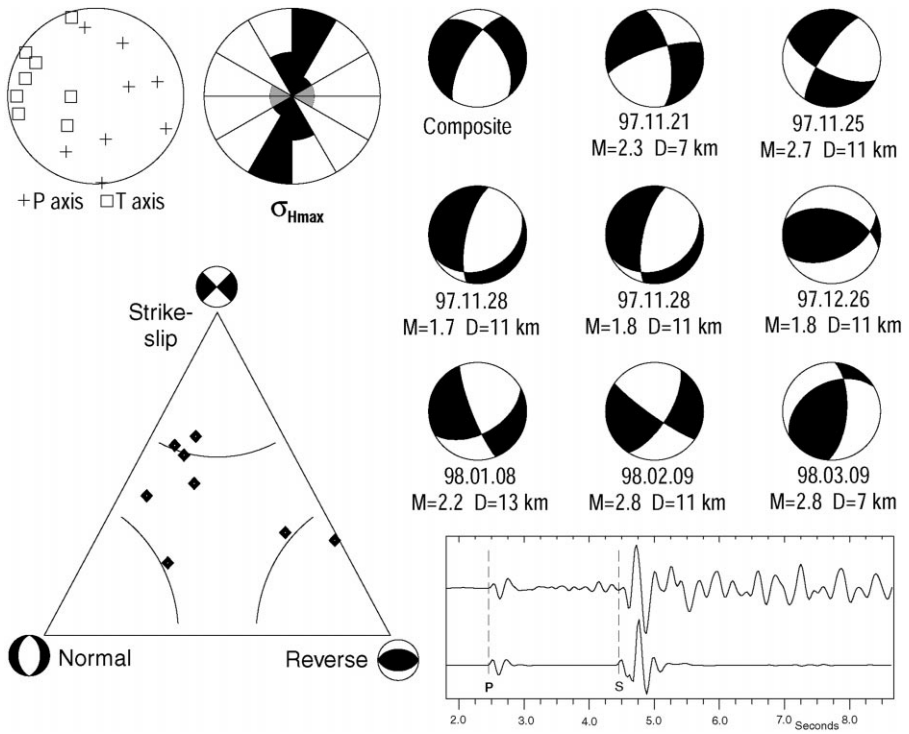


Fig. 4. The nine new earthquake focal mechanism solutions determined using data from the network. The composite solution uses first-motion polarities from 10 earthquakes, the other eight solution were determined using waveform modelling constrained by available first-motion polarities. The $P$ (compression) and $T$ (tension) axis for all solutions are plotted stereographically (upper left), showing that the $T$-axis (equivalent to $\sigma_3$; the minimum principal stress direction) are more consistent than the $P$-axis (corresponding to $\sigma_1$; the maximum principle stress). The directions of the maximum horizontal compressive stresses are plotted in the rose diagram (central left), showing a consistent NNE–SSW direction of horizontal compression. The two solutions outside the network (97.11.25 and 98.03.090) have clearly different $\sigma_{Hmax}$directions, and are plotted in grey. The actual focal mechanisms are shown on tripartite plots (lower left) where the three principal modes of faulting are connected to different corners in the triangles using the technique of Frohlich and Apperson (1992). At the bottom is shown a sample real (upper) and synthetic (lower) seismogram from one station, used in deriving the focal mechanism solution for the December 26, 1997, $M_L$ 1.8 earthquake. The P (compressional wave) and S (shear wave) phase arrivals are shown. The station was at a distance of 13 km from the earthquake hypocenter.

solutions generally comply well with other observed stress indicators and measurements, and also that they tend to be quite consistent on a regional scale (e.g., Bungum et al., 1991; Lindholm et al., 1995).

The most significant observation in Figs. 4 and 5 is that the directions of the largest horizontal compressive stress component are aligned subparallel to the coastline, which is close to a 90° rotation with respect to the

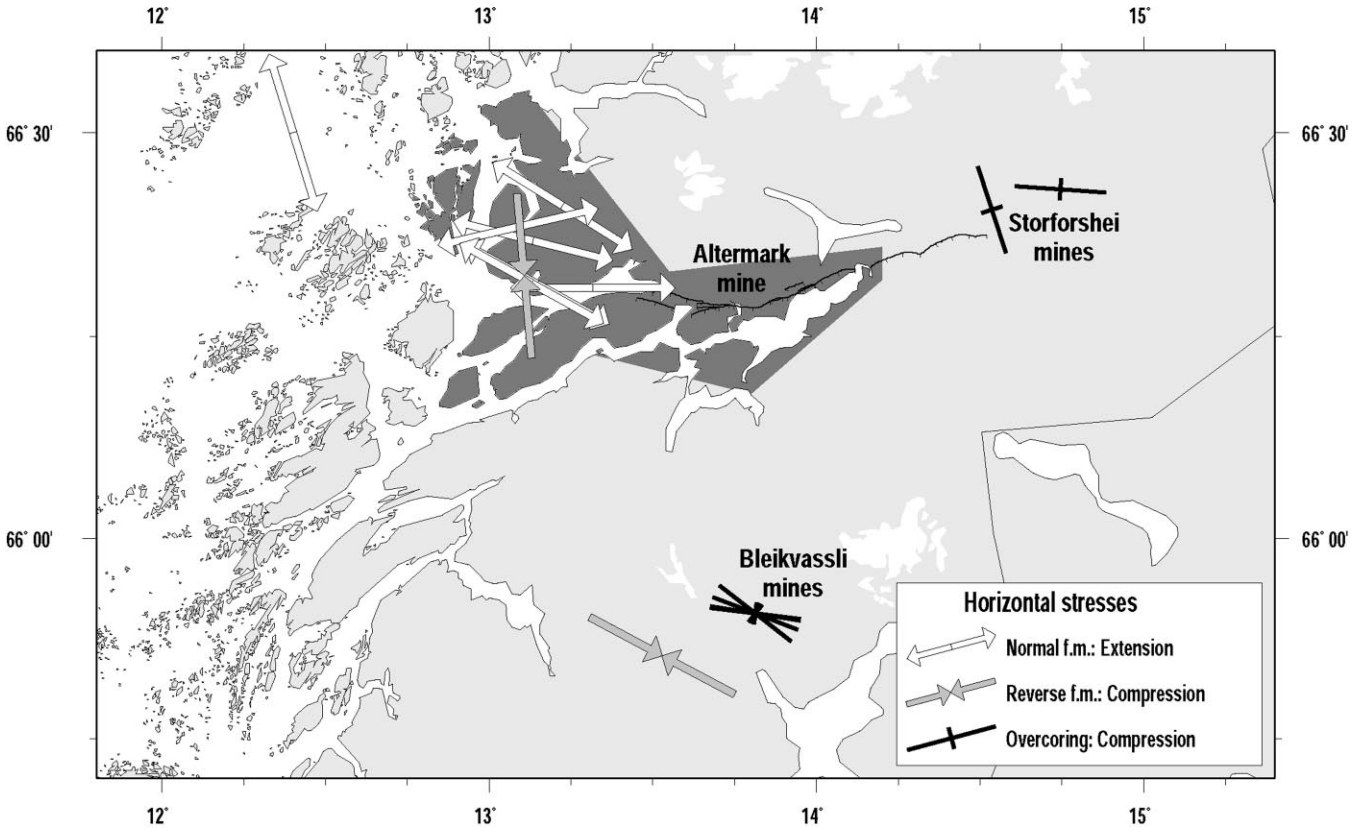


Fig. 5. Horizontal stresses from earthquake focal mechanism solutions and overcoring measurements in the Rana area. Normal faulting focal mechanism solutions are plotted as arrows in the direction of horizontal tension, while reverse solutions are plotted as arrows in the direction of horizontal compression. The overcoming measurements have the direction of maximum horizontal compression indicated by the symbol's long axis. The darker grey-shaded area represents the spatial extent of reported secondary ground effects (seiches, rockfalls, landslides, difficulties standing) from the 1819 $M_S$5.8–6.2 earthquake.

regional 'ridge push'-dominated trend. To describe these results in terms of maximum compressive stress is, however, deceptive since Fig. 4 shows (See also Table 1) that the solutions are predominantly normal to oblique normal/strike slip, and therefore are better described by the tensional stress component, running perpendicular to the coast. For this reason, the direction of horizontal tension is shown for the solutions with this classification in Fig. 5. Another important point is that the tensional component is much better constrained by this type of stress regime (Hicks et al., 2000), while the compressional axis is properly determined only in terms of its horizontal direction (as seen from Fig. 4), since its plunge may rotate more or less randomly, with a corresponding variation in the significance of the horizontal component. In conclusion, the data show a predominance of normal to strike-slip faulting in this region, with the tension axis oriented normal to the coast, the same direction as the compression axis in other areas.

A similar reversal of the main horizontal compressional axis has also been found in parts of the northern North Sea (Bungum et al., 1991; Lindholm et al., 1995, 2000; Hicks et al., 2000), in a region with very complex tectonics. In this case, however, the mode of faulting is more mixed and the reversal is also less prominent. It is important to note here that a switching of $\sigma_H$ and $\sigma_h$ (the largest and smallest horizontal stress component, respectively) is fairly easy to achieve when the $\sigma_H/\sigma_h$ ratio is close to unity, and it should be understood that this is therefore not as dramatic as is may at first appear. In this respect it is interesting to check this against in situ data, although the only available in situ data for this area are overcoring measurements from two mines (Storforshei mines and Bleikvassli mines, Fig. 5) taken at depths down to 400 m (Fejerskov et al., 1996). As for all in situ measurements, in this case especially due to the shallow depth of the measurements, the relation to the stress field at anything above the most local scale is uncertain. The horizontal stress anisotropy values of 1.1 for the Storforshei mines and four values between 1.2 and 1.7 for the Bleikvassli mines are not particularly close to unity, however, the measured anisotropy values are still low compared to many other mine overcoring measurements on the Norwegian mainland, where values above 2 are common.

A low horizontal stress anisotropy also raises the possibility that dilation effects (Barton, 1986) could have contributed to the observed stress rotation (Hicks et al., 2000). Such effects are based on the fact that dilation accompanying rock failure and weakness zone shearing introduces a component of shear strain that is no longer parallel to the assumed direction of shearing. The normal and shear stress changes that accompany dilatant shearing can radically alter the principal stress components that caused the event to occur, thereby potentially rotating major principal stresses (Nick Barton, pers. comm., 1999).

### 3.3. Magnitudes and depth distributions

The magnitude distribution as shown in Fig. 6 indicates that the detection threshold is about $M_L 0.9$. The detection threshold in the active areas near the Sjona fjord was most likely unchanged by the removal of two stations in October 1998 (see Fig. 2), due to the fact that the two closest stations were retained. The effect on location precision should be small, for the same reason.

The Gutenberg–Richter scaling relationship for earthquakes says that for a given region over a given period of time, the relation between number of earthquakes $N$ of magnitude equal to or greater than $M$ is given by

$$\log N = a - bM, \quad (1)$$

where the parameters $a$ and $b$ describe the activity level and the ratio between smaller and larger events, respectively. This has been applied to the local earthquake data to quantify the activity and magnitude scaling. The $a$ and $b$ values have been estimated as shown in Fig. 6, giving annual values of $a = 3.12$ and $b = 1.08$ (the latter being close to the commonly observed value of 1.0). This corresponds to a return period of 16 yr for earthquakes of magnitude $M_L 4$ or larger, 190 yr for $M_L 5$ and just under 2300 yr for $M_L 6$. Even though this is an excessive extrapolation, and $M_L$ is not properly defined at the level of magnitude 6, it still provides a rough indication of the activity in this area. These values could be compared to the regional activity levels as taken from a major seismic zonation study (NORSAR and NGI, 1998) developed for earthquake design purposes, which shows, albeit based on moment magnitudes, activity rate values $a = 3.0$ and $b = 1.05$ for a larger zone covering onshore Norway 66–68°N. This zone has return periods for magnitudes 4, 5 and 6 of 16, 180 and 2000 yr, respectively. This implies that the microearthquake activity in the Rana area, recorded only over 18 months, is quite consistent with the long-term ( $\sim$ 100 yr) average. If taken literally (that is, extrapolated linearly), these results indicate that the Rana area has a significant amount of the total seismic activity in onshore northern Norway.

The distribution of focal depths within the network is shown both in Figs. 3 and 6. The activity observed to the north of the Sjona fjord appears to have somewhat deeper hypocenter locations, with depths of about 8–12 km. The 51 earthquakes comprising the group by Handnesøya were located with hypocenter depths of about 6–8 km, but the witness reports of loud cracking and banging noises in conjunction with the earthquakes may indicate even shallower depths. As a consequence of the macroseismic reports, these events have been placed in the 3–5 km bin in Fig. 6, a depth range that is consistent with what has been found further north, in the Meløy region (Bungum et al., 1979).

It should be noted that most of the depths observed (2–6 km) are shallow compared to what is generally the

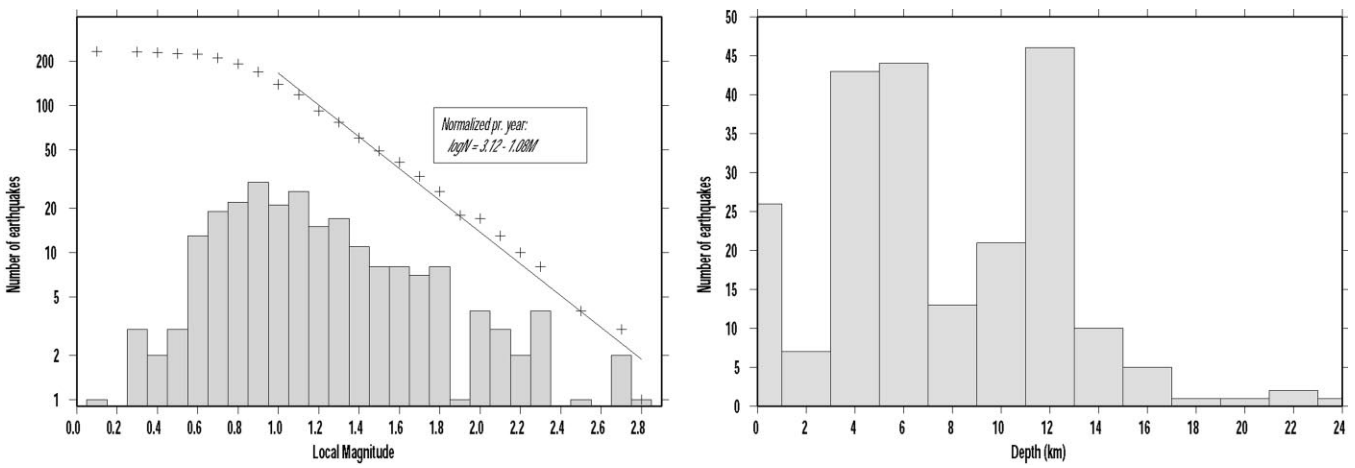


Fig. 6. (Left) Magnitude distribution for local events in the Rana area. Crosses represent the cumulative number of earthquakes. The activity rate (straight line) is defined using magnitude range $M_L$ 1.0–2.8. (Right) Depth distribution of earthquakes within the network. The majority if the events have hypocenter depths in the 3–7 km range, but with a large number also in the 9–13 km range. Note that the earthquakes with 0 km depths are due to insufficient data quality due to low magnitude and/or great distance, and should not be considered real.

case in Norway with offshore regions, and the slightly deeper earthquakes to the west and north of the Sjona fjord (8–12 km) are still considered shallow. Shallow seismic activity appear to be common for coastal areas in northern Norway where earthquake swarms (albeit with fairly normal *b*-values around 1.0) have also been observed earlier, notably in Meløy (Bungum et al., 1979, 1982a, b) and in Steigen (Atakan et al., 1994), as further discussed below. However, such swarms are not known from coastal areas further south.

It is interesting to note that similar swarms have also been documented in NW Scotland (Assumpção, 1981), on the Greenland margin (Gregersen, 1979, 1989; Chung and Gao, 1997), at Svalbard (Bungum et al., 1992; Mitchell et al., 1990), and at many locations in the Canadian Arctic, in particular the Sverdrup Basin (Smith et al., 1968; Basham et al., 1977; Wetmiller and Forsyth, 1978; Adams and Basham, 1991).

## 4. Discussion and conclusions

The local NEONOR network used in this study represents a significant improvement in terms of earthquake surveillance capability for this part of northern Norway. Even though a regional network has been in operation since 1987, with one station actually in the Rana region (MOR8 in Fig. 3), around 20% of the 267 local earthquakes analyzed here have been reported by the regional network. That network needs three stations to be detecting in order to report an event (Havskov et al., 1992), and has a detection threshold around $M_L$2.0 in the Rana area. Even then, the results found during these 18 months of operation are consistent with the more long-term seismicity models available, as suggested by the simple activity rate comparisons above.

The Rana area is the site of the largest historical earthquake known in Fennoscandia (and most likely also in northwestern Europe), namely the August 31, 1819 $M_S$5.8–6.2 earthquake (Muir-Wood, 1989a). This event created widespread ground effects in the Rana area, shown by the shaded area in Fig, 5, including standing waves (seiches) in fjords, numerous rockfalls and landslides, and reports of people having difficulties standing. It is notable that a large number of these effects were reported from the western parts of the present network (even though the villages were distributed fairly evenly along the Rana fjord), which is also where most of the present day seismic activity takes place. The exact location of the 1819 earthquake is, in spite of this, fairly poorly known, with estimates varying from the coastal region in the west to the Swedish border in the east. These locations are, however, mostly estimated from the isoseismal contours which extend throughout Fennoscandia (Muir-Wood and Woo, 1987). The problem with using the local secondary ground effects as indicated in Fig. 5 (as compared to the more distant isoseismal contours) in locating the event is that the population density is more dispersed east of Mo i Rana than farther west. Nevertheless, we believe that the local ground effects is strong evidence that the epicenter was in the area covered by the present study.

So, is the Rana region a persistent zone of enhanced seismic activity? Fig. 7 shows the spatial pattern of the instrumental earthquake locations from 1980 to 1997, and the new locations made using data from the NEONOR network. The instrumental locations between 1980 and 1997 are concentrated mainly in the western parts of the network, consistent with the new data. In contrast, a number of larger historic earthquakes (pre 1980) shown in Fig. 1 (a mix of macroseismic and instrumental locations) have locations further east, in an area just north of Mo i Rana. However, the location uncertainty for most of these earthquakes are of the order of 30–50 km (NORSAR and NGI, 1998), and some of these errors could also be systematic. In spite of these quality problems, however, the new data confirms that the Rana region as a whole is an area of continuos elevated seismic activity.

### 4.1. Geodynamic implications

Given the fact that the Rana area at large is seismically active, in relative terms, it is apparently surprising that none of this activity at present is directly connected to the Båsmoen fault itself (Dehls et al., 1998). However, this does not exclude the possibility that the fault has been active on a Holocene or historical time scale, even though the latter possibility now is less likely than earlier assumed. It is also uncertain if the large 1819 earthquake can be linked to any of the more NS-oriented structures that today's activity seems to define (cf. Fig. 3), even though a location in the same general area is likely, as discussed above. In this respect it is worth noting that magnitude 6 earthquake should normally be expected to nucleate deeper than the presently located shallow microearthquakes.

Local stress sources appear to play an important role in controlling the seismic activity in the Rana area, as evidenced by the apparent 90° rotation of the principal horizontal compression stress direction from the regional stress direction, which is commonly accepted to be plate tectonics related (Zoback, 1992; Hicks, 1996; Hicks et al., 2000). In general, the orientation of the maximum horizontal compressive stress as derived from earlier available onshore earthquake focal mechanism solutions in this region is more or less parallel to the coast (Byrkjeland et al., 2000). The focal mechanisms further west on the margin, however, have a NW–SE $\sigma_H$ orientation which is in compliance with the 'ridge push' direction. The majority of the earthquakes used to determine the regional stress field in mid Norway are located on the

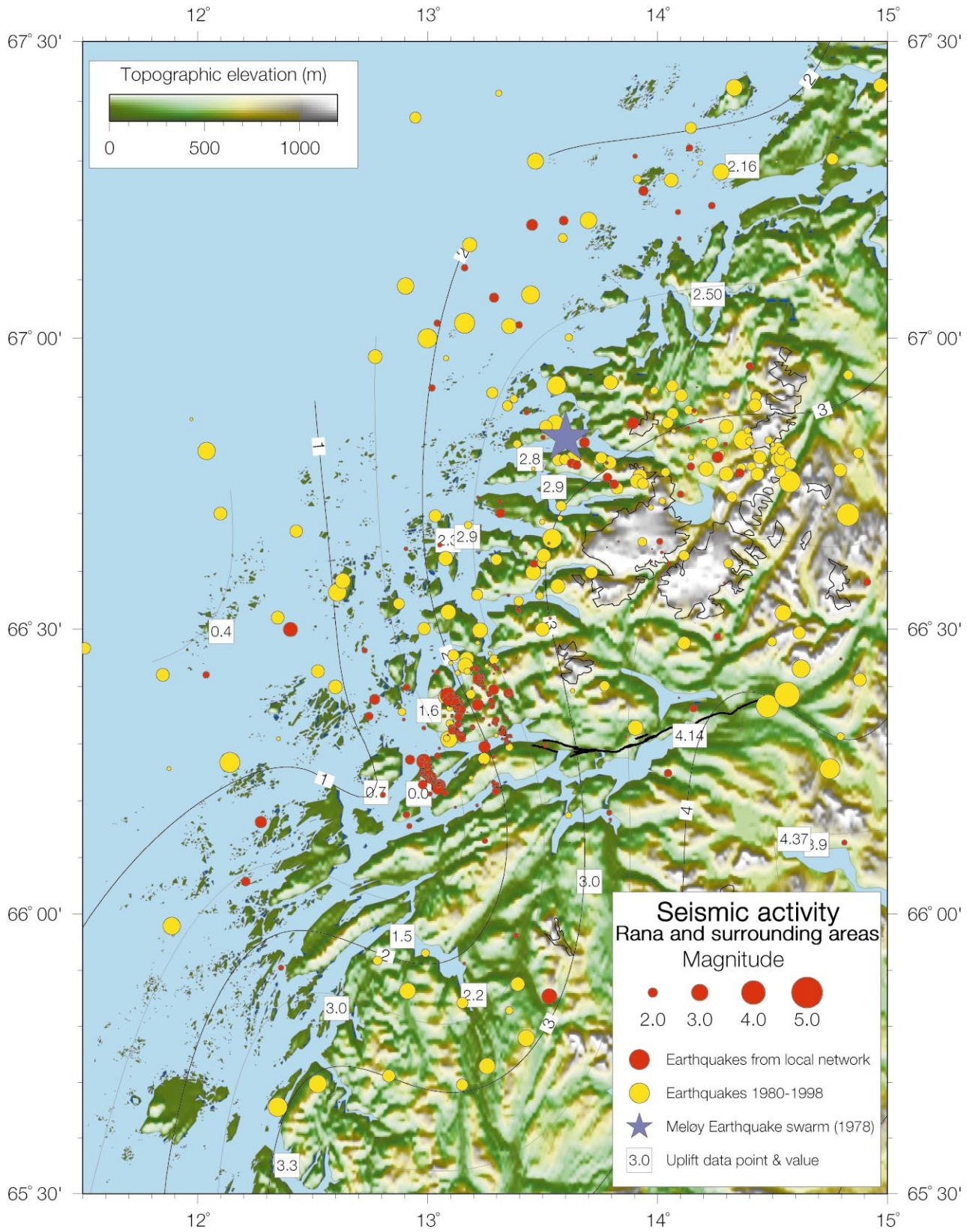


Fig. 7. New (August 1997–January 1999 — red) and instrumental (1980–1997 — yellow) earthquakes in northern central Norway. Contour lines for present-day uplift rates (mm $yr^{-1}$) are included, showing a clear anomaly in the western parts of the Rana fjord area. Data points and values used in the uplift grid are shown. The location of the Meløy earthquake swarm (Bungum et al., 1979) is given by the blue star. The 1819 earthquake has been located to the northwest northwest of Mo i Rana (Muir-Wood, 1989a), based on the large scale isoseismal intensity contours. However, due to the results presented in this paper, the epicenter is most likely located somewhat further west.

margin, so it may be inferred that such earthquakes are to a large degree, reflecting local second- and third-order sources of stress (density inhomogeneities, flexural stresses, topographic loads, geological features, etc.) rather than first-order (plate motion related) effects. This local control is also indicated by studies of the Meløy (Bungum et al., 1979) and the Steigen earthquake sequences (Atakan et al., 1994).

Several of these second-order sources of stress should be expected to generate stress perpendicular to the margin, to the coastline, and to the uplift trend, with potentials for both constructive and destructive interference. The fact that sediment flexure may create stresses one order of magnitude above those from ridge push, continental margin spreading and deglaciation flexure (Stein et al., 1989) means that this effect may dominate completely for offshore areas, as also concluded by Byrkjeland et al. (2000). Onshore this situation is different, however, and the point here is that what looks like a 90° rotation of the $\sigma_H$ direction in reality reflects normal-faulting mechanisms where the main tectonic significance is tied to the tensional axes, as discussed above and as plotted in Fig. 5. A tendency for more shallow normal-faulting earthquakes is also found onshore in southwestern Norway (Hicks et al., 2000).

As already noted, continental-side extension can result from both sediment flexure, density difference and spreading across continental margins, and from deglciation flexure. The two former sources of stress should, however, be expected to be of less importance in coastal areas, well into crystalline basement. This is also exactly where the post-glacial uplift gradients are at their highest (Fig. 1), pointing to that effect as more likely in this case than the other two. The two other well-documented coastal earthquake swarms in northern Norway (Meløy in 1978 and Steigen in 1992) also show similar patterns of shallow normal faulting with coast-normal extension. The geologic and tectonic setting for these swarms is similar to the Rana area. The main Meløy swarm (cf. Figs. 1 and 7) in 1978 consisted of around 10.000 earthquakes up to a magnitude of $M_L$3.2 during 10-week period (Bungum et al., 1979), based on temporary stations. The observed effect of the earthquakes by the local populace are also similar to those observed from the Handnesøya swarm in Rana, indicating similarly shallow depths. The Steigen swarm (cf. Fig. 1) consisted of 207 earthquakes in 1992 (Atakan et al., 1994) in several pulses. Hypocenter depths in this swarm are on the order of 8–11 km, again similar to some of the groups in the Rana area.

The two composite focal mechanism solutions available from the Meløy swarm show normal (Bungum et al., 1979) and strike-slip faulting (Vaage, 1980), the normal mechanism with coast-normal extension, and the strike-slip solution with the direction of horizontal compression around 45° to the coast. The focal mechanism solution (composite) available from the Steigen swarm is normal with coast-normal extension. The similarities between these two swarms and the seismic activity in the Rana area are striking, in terms of geologic setting, hypocenter depths, modes of faulting and post-glacial uplift gradients. There is also a single-event focal mechanism solution from an earthquake under the Lofoten Islands to the northwest (Hicks, 1996), indicating normal faulting with extension in the same direction as the Rana, Meløy and Steigen swarms. This argues that the stress sources responsible for the continuous high levels of seismic activity along the coast of northern Norway are effective on a scale of several hundred km, with post-glacial uplift being the most likely candidate. It is important to note in this context that the maximum post-glacial uplift gradients follow the coast quite closely (Fig. 1), adding further credibility to this hypothesis. Nevertheless, some influence of shorter-wavelength effects, such as topography and crustal inhomogeneities should also be considered due to the spatial concentration of the seismic activity. However, given the scarce nature and variable quality of the available seismic data in northern Norway, and also since many of the in situ stress orientations (albeit mostly from mines) show a NW–SE $\sigma_H$ axis, these problems call for further and strengthened investigations based on future acquisition and analysis of seismicity and stress data from the whole coastal region.

## 5. Conclusions

Given that the seismicity along the continental margin and in oceanic crust offshore Norway seems to be related to a combination of ridge push forces, sedimentation flexure and density differences and spreading across the margin, and region along the coast of northern Norway seems to behave differently seismically, as shown by the following conclusions that we can draw from the present study:

The Rana area has long been known as one of the more seismically active regions in Norway. The study confirms the continuous high level of seismic activity in this area, as the local seismic network has identified of the order of several hundred earthquakes within a limited area, with magnitudes up to $M_L$2.8. This is high for onshore Baltic shield areas.

The E–W-oriented Båsmoen fault did not reveal any seismic activity during the 18 month study period, which weakens but certainly does not exclude the possibility that this fault has been active during or after the last deglaciation. The consistency of the NNW–SSE lineations in the swarm-like activity in the five main groups of earthquakes in the western parts of the network, including a systematic change of depth, is significant, although the geological connection here is at present uncertain.

The tensional stress orientation perpendicular to the coastline combined with shallow foci leaves post-glacial uplift as a viable explanation for this seismicity, further supported by other earthquake source mechanisms farther north. Nevertheless, the very concentrated zones of activity are among the reasons why local sources of stress also could be influencing the occurrence of earthquakes in this region.

## Acknowledgements

The microseismic data used in this paper are provided by the NEONOR (Neotectonics in Norway) project, managed by the Norwegian Geological Survey, whom we also thank for providing geologic information. We also thank Dr. Iain Stewart and Dr. Robert Muir-Wood for constructive reviews of this paper.

## References

Adams, J., Basham, P.W., 1991. The seismicity and seismotectonics of eastern Canada. In: Slemmons, D.B., Engdahl, E.R., Zoback, M., Blackwell, D. (Eds.), Neotectonics of North America, Decade of North American Geology, Decade Map Volume 1, 261–276. Geological Society of America, Boulder, Colorado.

Alsaker, A., Kvamme, L.B., Hansen, R.A., Dahle, A., Bungum, H., 1991. The $M_L$ scale in Norway. Bulletin of the Seismological Society of America 81, 379–398.

Andersen, B.G., 1975. Glacial geology of northern Nordland, North Norway. Norges Geologiske Undersøekelse 320, 1–74.

Andersen, B.G., Bøen, F., Rasmussen, A., Rokoengen, K., Vallevik, P.N., 1982. The Tjøtta glacial event in southern Nordland, North Norway. Norsk Geologisk Tidsskrift 62, 39–49.

Andersen, B.G., Mangerud, J., Sørensen, R., Reite, A., Sveian, H., Thoresen, M., Bergstrøm, B., 1995. Younger Dryas ice-marginal deposits in Norway. Quaternary International 28, 147–169.

Atakan, K., Lindholm, C.D., Havskov, J., 1994. Earthquake swarm in Stgeigen, northern Norway: an unusual example of intraplate seismicity. Terra Nova 6, 180–194.

Assumpção, M., 1981. The NW Scotland earthquake swarm of 1974. Geophysical Journal of the Royal Astronomical Society 67, 577–586.

Bäckblom, G., Stanfors, R., 1988. Interdisciplinary study of postglacial faulting in the Lensjärv area, northern Sweden 1986–1988. SKB Technical Report 89–31.

Basham, P.W., Forsyth, D.A., Wetmiller, R.J., 1977. The seismicity of northern Canada. Canadian Journal of Earth Sciences 14, 1646–1667.

Bergstrøm, B., 1994. ERLSFJORD. Kvartærgeologisk kart 1927 III-M 1:50000, med beskrivelse (Quaternary geology map with description). Norges Geologiske Undersøekelse.

Blake, K.P., Olsen, L., 1999. Deglaciation of Svartisen area, northern Norway, and isolation of a large ice mass in front of the Fennoscandian Ice Sheet. Norsk Geologisk Tidsskrift 53, 1–16.

Bott, M.H.P., 1991. Ridge push and associated plate interior stress in normal and hot spot regions. Tectonophysics 200, 17–23.

Bott, M.H.P., Kusznir, N.J., 1984. The origin of tectonic stress in the lithosphere. Tectonophysics 105, 1–13.

Bungum, H., Alsaker, A., Kvamme, L.B., Hansen, R.A., 1991. Seismicity and seismotectonics of Norway and surrounding continental shelf areas. Journal of Geophysical Research 96, 2249–2265.

Bungum, H., Hokland, B.K., Husebye, E.S., Ringdal, R., 1979. An exceptional intraplate earthquake sequence in Meløy, Northern Norway. Nature 280, 32–35.

Bungum, H., Lindholm, C., 1997. Seismo- and neotectonics in Finnmark, Kola Peninsula and the southern Barents Sea. Part 2: Seismological analysis and seismotectonics. Tectonophysics 270, 15–28.

Bungum, H., Mitchell, B.J., Kristoffersen, Y., 1982a. Concentrated earthquake zones in Svalbard. Tectonophysics 81, 175–188.

Bungum, H., Vaage, S., Husebye, E.S., 1982b. The Meløy earthquake sequence, northern Norway: source parameters and their scaling relations. Bulletin of the Seismological Society of America 72, 197–206.

Byrkjeland, U., Bungum, H., Eldholm, O., 2000. Seismotectonics of the Norwegian continental margin. Journal of Geophysical Research 105, 6221–6236.

Chung, W.-Y., Gao, H., 1997. The Greenland earthquake of 11 July 1987 and postglacial fault reactivation along a passive margin. Bulletin of the Seismological Society of America 87, 1058–1068.

Dahlen, F.A., 1981. Isostasy and the ambient state of stress in the oceanic lithosphere. Journal of Geophysical Research 86, 7801–7807.

Dehls, J., Olesen, O. 1998. Neotectonics in Norway, Annual Technical Report 1997, NGU (Norges Geologiske Undersøkelse) Report 98.016, 149 pp.

Dehls, J., Olesen, O. 1999. Neotectonics in Norway, Annual Technical Report 1998, NGU (Norges Geologiske Undersøkelse) Report 2000.001.

Dehls, J., Olesen, O., 2000. Neotectonics in Norway, Annual Technical Report 1999, NGU (Norges Geologiske Undersøkelse) Report 00.xxx.

Dehls, J., Olesen, O. Olsen, L., Blikra, L.H., 2000. Neotectonic faulting in northern Norway: the Stuoragurra and Nordmannvikdalen postglacial faults. In: Stewart, I.S., Sauber, J., Rose, J. (Eds), Glacioseismotectonics: Ice Sheets, Crustal Deformation and Seismicity. Quaternary Science Reviews, this issue.

Denton, G.H., Hughes, T.J., 1981. The Last Great Ice Sheets. Wiley, New York.

Ekman, M., 1996. A consistent map of the postglacial uplift of Fennoscandia. Terra Nova 8, 158–165.

Fejerskov M., Lindholm, C. 2000. Crustal stress in and around Norway; An evaluation of stress generating mechanisms. In: Nøttredt, A. et al. (Eds), Dynamics of the Norwegian Margin. Geological Society of London, Special Publications 167, 451–467.

Fejerskov, M., Lindholm, C.D., Bungum, H., Myrvang, A., Bratlie, R.K., Larsen, B.T., 1996. Crustal stress in Norway and adjacent offshore regions. Final Report for the IBS-DNM project, Topic 1.3 "Regional stress field".

Fjeldskaar, W., 1994. Viscosity and thickness of the astenosphere detected from the Fennocandian uplift. Earth and Planetary Science Letters 126, 399–410.

Fjeldskaar, W., 1997. Flexural rigidity of the Fennoscandia inferred from the postglacial uplift. Tectonics 16, 596–608.

Frohlich, C., 1982. Seismicity of the central gulf of Mexico. Geology 10, 103–106.

Frohlich, C., Apperson, K.D., 1992. Earthquake focal mechanisms, moment tensors, and the consistency of seismic activity near plate boundaries. Tectonics 11, 279–296.

Gjelle, S., Bergstrøm, B., Gustavson, M., Olsen, L., Sveian, H., 1995. Geology and landscape around the Arctic Circle in Norway. Weenebergs trykkeri AS, Trondheim, 128 pp.

Gregersen, S., 1979. Intraplate earthquake swarms in Greenland and adjacent continental regions. Nature 281, 661–662.

Gregersen, S., 1989. The seismicity of Greenland. In: Gregersen, S., Basham, P.W. (Eds.), Earthquakes at North-Atlantic passive margins: Neotectonics and Postglacial Rebound, NATO ASI Series, Vol. 266, pp. 345–353. Kluwer Academic Publications, Dordrecht.

Gregersen, S., 1992. Crustal stress regime in Fennoscandia from focal mechanisms. Journal of Geophysical Research 97, 11821–11827.

Havskov, J., Kvamme, L.B., Hansen, R.A., Bungum, H., Lindholm, C.D., 1992. The northern Norway seismic network: design, operation and results. Bulletin of the Seismological Society of America 82, 481–496.

Hermann R.B., 1987. Computer Programs in Seismology, Vol. I-VII. Saint Louis University, St. Louis, Missouri.

Herrmann, R.B., Wang, C.Y., 1985. A comparison of synthetic seismograms. Bulletin of the Seismological Society of America 75, 41–56.

Hicks, E.C., 1996. Crustal stresses in Norway and surrounding areas as derived from earthquake focal mechanisms and in-situ stress measurements. Cand. Scient Thesis in Applied Geophysics, University of Oslo, Norway, 163 pp.

Hicks, E., Bungum, H., Lindholm, C., 2000. Stress inversions of earthquake focal mechanism solutions from onshore and offshore Norway. Norsk Geologisk Tidsskrift, submitted for publication.

Johnston, A.C., 1987. Suppression of earthquakes by large continental ice sheets. Nature 330, 467–469.

Johnston, A.C., Coppersmith, K.J., Kanter, L.R., Cornell, C.A., 1994. The earthquakes of stable continental regions. Technical Report, EPRI TR-1022261s-V1-V5, Electr. Power Res. Inst., Palo Alto, CA, 1994.

Johnston A.C., Kanter, L.R., 1990. Earthquakes in stable continental crust. Scientific American, March 1990, 42–49.

Johnston, P., Wu, P., Lambeck, K., 1998. Dependence of horizontal stress magnitude on load dimension in glacial rebound models. Geophysical Journal International 132, 41–60.

Lindholm, C., Bungum, H., Bratlie, R.K., Aadnøy, B.S., Dahl, N., Tørudbakken, B., Atakan, K., 1995. Crustal stress in the northern North Sea as inferred from in situ measurements and earthquake focal mechanisms. Terra Nova 7, 51–59.

Lindholm, C.D., Bungum, H., Hicks, E., Villagran, M. 2000. Crustal stress and tectonics in Norwegian regions determined from earthquake focal mechanisms. In: Nøttredt, A. et al. (Eds), Dynamics of the Norwegian Margin. Geological Society London, Special Publications 167, 429–439.

Lundquist, J., Lagerbäck, R., 1976. The Pärve fault, A late-glacial fault in the Precambrian of Swedish Lapland. Geologiska Foereningens i Stockholm Foerhandlingar 98, 45–51.

McKenzie, D.P., 1969. The relation between fault plane solutions for earthquakes and the directions of the principal stresses. Bulletin of the Seismological Society of America 59, 591–601.

McNutt, M.K., Menard, H.W., 1982. Constraints on yield strength in the oceanic lithosphere derived from observations of flexure. Geophysical Journal of the Royal Astronomical Society 71, 363–394.

Mitchell, B.J., Bungum, H., Chan, W.W., Mitchell, P.B., 1990. Seismicity and present-day tectonics of the Svalbard region. Geophysical Journal International 102, 139–149.

Muir-Wood, R., 1989a. The Scandinavian earthquakes of 22 December 1759 and 31 August 1819. Disasters 12, 223–236.

Muir-Wood, R., 1989b. Extraordinary deglaciation reverse faulting in northern Fennoscandia. In: Gregersen, S., Basham, P.W. (Eds.), Earthquakes at North-Atlantic passive margins: Neotectonics and Postglacial Rebound, NATO ASI Series, Vol. 266 pp. 141–174. Kluwer Academic Publications, Dordrecht.

Muir-Wood, R., 1993. A review of the seismotectonics of Sweden. EQE International, Report: 43-01-R-001, Revision 2, 1993.

Muir-Wood, R., Woo, G., 1987. The historical seismicity of the Norwegian Continental Shelf. ELOCS (Earthquake Loading on the Norwegian Continental Shelf) Report 2-1, Norwegian Geotechnical Institute, Oslo.

NORSAR and NGI, 1998. Seismic Zonation for Norway. Report prepared for the Norwegian Council for Building Standardization (NBR), 188 pp.

Olesen, O., 1988. The Stuoragurra fault, evidence of neotectonics in the Precambrian of Finnmark, northern Norway. Norsk Geologisk Tidsskrift 68, 107–118.

Olesen, O., Hjelle, S., Henkel, H., Karlsen, T.A., Olsen, L., Skogseth, T., 1994. Neotectonics in the Ranafjorden area, northern Norway. NGU (Norges Geologiske Undersøekelse) Report No. 94.073, 33 pp.

Olsen, L., Sveian, H., Blikra, L.H., 1996. KORGEN 1927 II – M 1:50000, Kvartærgeologisk kart med beskrivelse (Quaternary geology map with description). Norges Geologiske Undersøekelse.

Rasmussen, A., 1981. The deglaciation of the coastal area NW of Svartisen, Northern Norway. Norges Geologiske Undersøekelse 369, 1–31.

Smith, W.E.T., Whitham, K., Piche, W.T., 1968. A microearthquake swarm in 1965 near Mould Bay, Northwest Territories, Canada. Bulletin of the Seismological Society of America 58, 1991–2011.

Sibson, R.H., 1985. A note on fault reactivation. Journal of Structural Geology 7 (6), 751–754.

Stein, S., Cloetingh, S., Sleep, N.H., Wortel, R., 1989. Passive Margin Earthquakes, Stresses and Rheology. In: Gregersen, S., Basham P.W. (Eds.), Earthquakes at North-Atlantic passive margins: Neotectonics and Postglacial Rebound, NATO ASI Series, Vol. 266. pp. 231–259. Kluwer Academic Publications, Dordrecht.

Stephansson, O., 1988. Ridge push and glacial rebound as rock stress generators in Fennoscandia. Bull. 14, Geol. Inst., Univ. of Uppsala, Sweden, pp. 39–48.

Vaage, S., 1980. Seismic evidence of complex tectonics in the Meløy earthquake area. Norsk Geologisk Tidsskrift 60, 213–217.

Walcott, R.I., 1970. Flexural rigidity, thickness, and viscosity of the lithosphere. Journal of Geophysical Research 75, 3941–3954.

Wetmiller, R.J., Forsyth, D.A., 1978. Seismicity of the Arctic, 1908–1975. Publs. Earth Physics Br. 45, 15–24.

Wu, P., Hasegawa, H., 1996. Induced stresses and fault potential in eastern Canada due to a realistic load: a preliminary analysis. Geophysical Journal International 127, 215–229.

Zoback, M.L., 1992. First- and second-order patterns of stress in the lithosphere. The World Stress Map Project. Journal of Geophysical Research 97, 11703–11728.